Potential flow in the presence of a sudden expansion: Application to capillary driven transport in porous media

Eric M. Benner and Dimiter N. Petsev*

Department of Chemical and Nuclear Engineering, University of New Mexico, Albuquerque, New Mexico 87131, USA

(Received 13 September 2012; published 13 March 2013)

We present a theoretical analysis of the capillary driven transport of liquid in porous media that undergoes a sudden expansion. The use of appropriate coordinates allows for exactly and analytically solving different cases in two and three dimensions. The time dependence of liquid front motion in an expanding porous media is shown to be different from the one-dimensional Lucas-Washburn [Lucas, Kolloid Z. **23**, 15 (1918); Washburn, Phys. Rev. **17**, 273 (1921)] results as well as from the solution for two- and three-dimensional circular expansions obtained by Hyväluoma *et al.* [Phys. Rev. E **73**, 036705 (2006)] and Xiao *et al.* [Langmuir **28**, 4208 (2012)]. These cases appear as asymptotic limits of our solutions. We also observe that capillary flow in expanding three-dimensional porous materials exhibits a steady state solution for the bulk flow rate at the entrance of the expansion.

DOI: 10.1103/PhysRevE.87.033008 PACS number(s): 47.56.+r, 47.15.km, 47.55.nb, 47.85.Np

I. INTRODUCTION

Capillary driven liquid flows in porous media are ubiquitous phenomena that occur both in nature and in various practical applications [1–8]. The dynamics of such flows was first analyzed about a century ago [9–11] for the simple case of one-dimensional transport in porous materials (or capillaries) of uniform cross section. The advancement of the liquid is driven by the capillary pressure due to the curvature of the liquid-gas interface in each individual pore. Hence the liquid should wet the pore walls with a contact angle that is less than 90°. As the liquid penetrates further into the porous material of constant cross section, the total hydrodynamic resistance increases and the bulk flow rate decreases proportionally to $t^{-1/2}$ (where t is time). This result is often referred to as the Lucas-Washburn (LW) relationship [10,11]. The LW model was strictly derived for the flow in a single straight capillary. For a porous media the LW relationship has an average macroscopic meaning, similar to the Darcy equation [6,12] with pressure drop determined by capillarity and a permeability coefficient that is a complex function of the porosity. The LW model is based on the assumption that the flow is governed by the liquid motion, and the displacement of the gas phase at the front does not practically contribute due to its much lower dynamic viscosity. The model assumes a single-phase system with a moving front, and is valid in the limit of small gas pressure and density. This has been both experimentally and theoretically shown to be reasonable for a great number of systems involving liquids moving in porous media [4,6,13–18], including by carefully obtaining the density profile at the front [19]. In the case of two immiscible liquids displacing each other, the flow needs to be treated as a two-phase liquid and will depend on both viscosities [6]. The focus of the present paper is on liquid phase capillary flow in porous materials without entrapment of air anywhere in the wetted region.

The time behavior of liquid penetration in porous media is very different if the flow occurs in porous media that expands (or contracts) in the direction of the flow. Estimations of the bulk flows in two- (2D) and three-dimensional (3D) expanding porous media were offered [13–15] suggesting that the time dependence of the flow deviates from the LW one-dimensional (1D) case. The cases of 2D radial flow where the front is represented by a gradually expanding circle were analyzed in detail by Hyväluoma *et al.* [17]. The authors compared the capillary driven flow Darcy-type model to lattice-Boltzmann simulation and obtained excellent agreement, thus validating the analytical approach. The detailed analysis of the 3D case corresponding to an expanding spherical surface was performed by Xiao *et al.* [16]. There the capillary driven transport model was tested against carefully performed experiments and again both were found to be in agreement. To maintain circular or spherical symmetries the flows must start from a point or an already circular (for 2D) or spherical (3D) boundary. Hyväluoma *et al.* [17] used the model to describe the penetration of liquid in two dimensions from a droplet with circular circumference sitting on porous paper. They showed that the liquid velocity decreases with time following a different and more complicated dependence. Xiao *et al.* [16] used the spherical expansion model to fit experimental data on capillary penetration of water in packed glass beads. All these results are very important because they imply that the shape of the porous material leads to qualitative differences in the resulting flow patterns. This means that applications using capillary driven transport in porous media can be optimized by simply shaping the materials accordingly [4].

In this paper we present exact analytical results for the flow in porous media that exhibit sudden expansion (see Fig. 1). The flow in these cases is not necessarily radial as in the Refs. [16,17] because the entrance to the expanding porous space has finite dimensions and is usually flat instead of circular. Our results include a linear velocity field at each point (on a scale greater than the typical average pore size) in the domain of interest. The detailed knowledge of the local fluid velocity is very important for applications like designing paper based diagnostic devices with different shapes [2,4], delivering solutions to power fuel cells [8], or to better understanding how moisture penetrates construction materials [13,14]. We derive the position of the wetted front as well as the bulk flow rate in

*Corresponding author: Dimiter@unm.edu

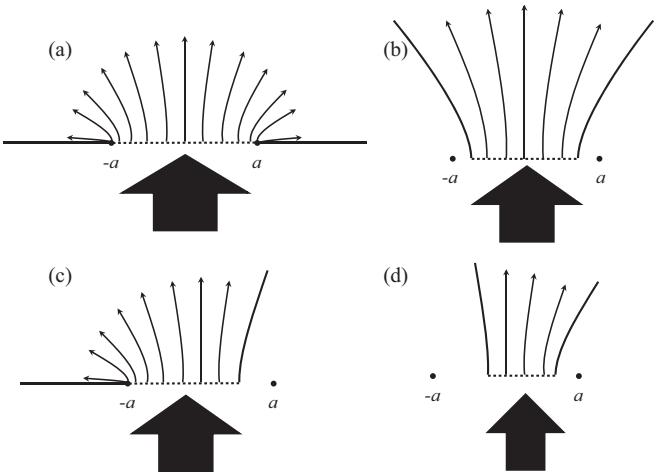

FIG. 1. Examples for flows in various types of expanding porous media in 2D cases [see Eqs. (5) and Fig. 2.] Case (a) corresponds to $0 \leqslant \psi \leqslant \pi$. Case (b) corresponds to $\psi_1 \leqslant \psi \leqslant \pi - \psi_1$ where ψ_1 is an arbitrary angle. Case (c) corresponds to $\psi_1 \leqslant \psi \leqslant \pi$. Case (d) corresponds to $\psi_1 \leqslant \psi \leqslant \pi/2$. Rotating cases (a) and (b) around the y axis gives a 3D flow in expanding media [see Eqs. (29) and Fig. 3] with $0 \leqslant \theta \leqslant \pi/2$ and $0 \leqslant \theta \leqslant \theta_1$, respectively, where θ_1 is an arbitrary angle.

the porous material as functions of the elapsed time. The 2D solution is applicable to a wide variety of shapes. The 3D case can be simply treated only if the domain has axial symmetry. We will limit our analysis only to porous domains with zero flow across the side boundaries and will ignore inertia effects. Inertia and hydrodynamic nonlinearity are important in the initial moment of liquid penetration into the porous media and depend on the driving capillary pressure [20]. The latter is a function of the pore (capillary) radius and the wetting contact angle. As the pores may vary in size, the capillary pressure used in our model is an average over the pore size distribution, which has to be sufficiently narrow to prevent capillary fingering from occurring. It has been shown that for radii of the order of 50 μm inertia is usually important. If the wetting contact angle is 0° then inertial terms might be significant down to 10 μm pore radii [20]. Below these pore sizes viscosity is dominant and inertia does not play a role. The solution is restricted to the assumption that gravitational effects are negligible. For approximately 2D systems this is usually reasonable, even for large systems, as the dimensions are commonly orthogonal to the gravitational field. However, in 3D systems this means that the solution degrades as the total weight of the fluid in the medium approaches the interfacial contact length times the surface tension (i.e. the Bond number grows) because this greatly distorts the front of the advancing fluid by gravitational percolation [15]. Finally, our analysis does not include possible evaporation of 2D surfaces or of the side boundaries for both 2D and 3D systems. The analysis of cases with permeable side boundaries and surface evaporation will be published elsewhere [21].

In the next section, we present a general overview of the capillary driven flow in porous materials. Section III presents the derivation of results for the flow velocity in 2D expanding porous media, Sec. IV presents the solution for the capillary driven flow in an expanding 3D porous material, Sec. V discusses and compares the results for each of the respective geometries, and Sec. VI summarizes the conclusions.

II. GOVERNING EQUATIONS FOR THE FLOW IN POROUS MEDIA

The flow of incompressible liquid in porous media is given by the mass balance

$$\nabla \cdot \mathbf{v} = 0, \tag{1}$$

where $\mathbf{v}$ is the linear liquid velocity on a scale that is larger than the individual pore size. For mass flux a sink or source term, Q, (e.g., evaporation, condensation, etc.) may be added to the right-hand side of Eq. (1); this term is presently ignored. The liquid flow in porous media is irrotational [22]; therefore the velocity can be expressed by means of the velocity potential, φ,

$$\mathbf{v} = \nabla\varphi = -\frac{k}{\mu}\nabla P, \quad \varphi = -\frac{k}{\mu}P. \tag{2}$$

The right-hand side of Eq. (2) is Darcy's law [12,22] where k is the permeability of the medium, μ is the dynamic shear viscosity of the liquid, and P is the pressure that drives the flow. In the case of capillary driven flow the pressure is equal to

$$P_C = \gamma \cos\alpha \left(\frac{1}{R_1} + \frac{1}{R_2}\right), \tag{3}$$

where γ is the interfacial tension at the gas-liquid interface and α is the contact angle that characterizes the wetting of the solid [23]. R_1 and R_2 are the two principal radii of curvature of the pore. Equations (1) and (2) can be combined to give

$$\nabla^2\varphi = 0. \tag{4}$$

Equation (4) will be used to obtain expressions for the liquid flow in all cases analyzed below.

III. CAPILLARY DRIVEN FLOW IN TWO-DIMENSIONAL EXPANDING POROUS MEDIA

A. Exact solution in two dimensions

Different examples illustrating capillary liquid transport in expanding 2D porous media are sketched in Fig. 1. Figures 1(a) and 1(b) show symmetric regions with different extent of expansion. Figures 1(c) and 1(d) represent two asymmetric cases. The liquid enters the expanding region through an entrance with finite width. Because of the finite size of the entrance, the shape of the expanding liquid front is elliptical rather than circular as in the case discussed by Hyväluoma *et al.* [17]. The entrance is saturated with liquid and the pressure there equals the ambient. The front of the moving wetted region is where the liquid meets the gas phase in the pores and the pressure there is equal to the ambient minus the capillary pressure [see Eq. (3)]. Hence, we look for a solution in the domain that starts at the entrance and propagates a wetted front. The problem is best defined in elliptic coordinates [24] (see Fig. 2),

$$x = a\cosh\eta\cos\psi, \quad y = a\sinh\eta\sin\psi. \tag{5}$$

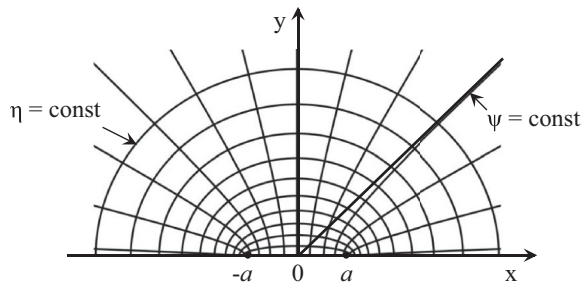

FIG. 2. Elliptic coordinates, used to describe the flow in an expanding 2D porous domain. The points $-a$ and a are the foci of the ellipses.

The general form of Eq. (4) then becomes

$$\nabla^2\varphi = \frac{1}{a^2(\cosh^2\eta - \cos^2\psi)}\left(\frac{\partial^2\varphi}{\partial\eta^2} + \frac{\partial^2\varphi}{\partial\psi^2}\right) = 0. \quad (6)$$

If there is no liquid flow across the edges of the domain that are defined by $\psi = \psi_1$ and $\psi = \psi_2$ (see Fig. 1), there will be no variation of φ with respect to the angular variable ψ. Hence the term $\partial^2\varphi/\partial\psi^2$ can be dropped from Eq. (6) and the equation simplifies to

$$\frac{d^2\varphi}{d\eta^2} = 0. \quad (7)$$

The solution of this equation describes concentric elliptic lines that correspond to the flow potential φ at a given η. The boundary conditions are

$$\varphi = \varphi_0 = -\frac{k}{\mu}P_C \quad \text{at} \quad \eta = 0, \quad \varphi = 0 \quad \text{at} \quad \eta = \eta_f, \quad (8)$$

where $\eta = 0$ at the entrance and $\eta = \eta_f$ at the front. The solution of Eq. (7) is then

$$\varphi = -\frac{k}{\mu}P_C\left[1 - \frac{\eta}{\eta_f}\right]. \quad (9)$$

Hence the velocity of the moving liquid is

$$v_\eta = (\nabla\varphi)_\eta = \frac{1}{a(\cosh^2\eta - \cos^2\psi)^{1/2}}\frac{\partial\varphi}{\partial\eta} = \frac{1}{a(\cosh^2\eta - \cos^2\psi)^{1/2}}\left(\frac{kP_C}{\mu}\frac{1}{\eta_f}\right). \quad (10)$$

Following the approach outlined by Washburn [11], we derive an equation for the velocity of the moving front,

$$v_{\eta_f} = a(\cosh^2\eta_f - \cos^2\psi)^{1/2}\frac{d\eta_f}{dt} = \frac{1}{a(\cosh^2\eta_f - \cos^2\psi)^{1/2}}\left(\frac{\partial\varphi}{\partial\eta}\right)_{\eta=\eta_f} = \left(\frac{kP_C}{a\mu}\right)\frac{1}{(\cosh^2\eta_f - \cos^2\psi)^{1/2}}\frac{1}{\eta_f}. \quad (11)$$

For plotting it is convenient to use a dimensionless velocity that has the form $\tilde{v}_{\eta_f} = (\mu a/kP_C)\,v_{\eta_f}$.

The time dependence of the position of the liquid front $\eta_f(t)$ can be derived by integrating Eq. (11):

$$\frac{kP_C}{\mu}\int_0^{\eta_f(t)}\frac{(\cosh^2\eta'_f - \cos^2\psi)}{(\partial\varphi/\partial\eta)_{\eta=\eta'_f}}d\eta'_f = \tilde{t}, \quad \tilde{t} = \frac{kP_C}{\mu a^2}t. \quad (12)$$

After integration and brief rearrangement Eq. (12) leads to the following relationship for the time-dependent position of the liquid front:

$$\eta_f\sinh(2\eta_f) - \tfrac{1}{2}\cosh(2\eta_f) - \cos(2\psi)\eta_f^2 + \tfrac{1}{2} = 4\tilde{t}. \quad (13)$$

Equation (13) represents the dependence of the front position on time $\eta_f(\tilde{t})$. Differentiating with respect to time and multiplying it by the factor $a(\cosh^2\eta_f - \cos^2\psi)^{1/2}$ gives the time-dependent velocity of the front [see the top line of Eq. (11)]. Alternatively $\eta_f(\tilde{t})$ can be introduced in the last line of Eq. (11) to obtain the time dependence of the linear velocity $\tilde{v}_f(\tilde{t})$.

Another quantity of interest is the volumetric flux of liquid through the entrance, U. It is equal to the integral over the liquid linear flow velocity across the area of the front, or [see Eq. (11)]

$$U(\tilde{t}) = \int_A \mathbf{v}\cdot\mathbf{n}dA = a\int_{\psi_1}^{\psi_2} v_{\eta_f}(\tilde{t})[\cosh^2\eta_f(\tilde{t}) - \cos^2\psi]^{1/2}d\psi = \left[\frac{kP_C}{\mu\eta_f(\tilde{t})}\right](\psi_2 - \psi_1). \quad (14)$$

Since the liquid motion occurs in the 2D plane, the above result is per unit length in direction normal to the plane surface. The local linear velocity $\tilde{v}$ will decrease with the increase of η in an expanding domain and is lowest at the front where $\eta = \eta_f$. The volumetric flux, U, conserves because as the linear velocity decreases the front area increases to exactly compensate. Both, however, will change with time. For a fully open entrance ($\psi_1 = 0, \psi_2 = \pi$) one obtains

$$U(\tilde{t}) = \frac{\pi kP_C}{\mu\eta_f(\tilde{t})}. \quad (15)$$

B. Asymptotic results for small and large η_f

For short times, η_f is small and we can further simplify the solution (13) (also setting $\psi = \pi/2$) to read

$$\frac{\eta_f^2}{2} = \tilde{t}. \quad (16)$$

This expression is formally identical to the LW result [10,11],

$$\frac{L(t)^2}{2a^2} = \tilde{t}, \quad (17)$$

which describes the position of the front $L(t)$ in a porous domain with constant cross section. Hence for short times and small η_f the effect of the expansion is negligible. It is also important to stress that the short times discussed here are reflecting only the effect of the porous media geometry and are

still long in comparison to the time scale of any inertial fluid motion. Inertia (if present) occurs on a time scale that is much faster (about a fraction of a second) and practically absent for pores with radii below 10 μm, or for even larger pores if the wetting contact angle is less than 0° [20].

The asymptotic result for large η_f is obtained by realizing that $\sinh(2\eta_f) \to \exp(2\eta_f)/2$ and $\cosh(2\eta_f) \to \exp(2\eta_f)/2$. At long times the asymptotic result for Eq. (13) is

$$\tfrac{1}{8}\eta_f \exp(2\eta_f) - \tfrac{1}{16}\exp(2\eta_f) = \tilde{t}. \tag{18}$$

As will be shown below, Eq. (18) is identical to the long-time asymptotic results of Hyväluoma *et al.* [17],

$$\left(\frac{R_f}{R_0}\right)^2 \ln\left(\frac{R_f}{R_0}\right)^2 - \left(\frac{R_f}{R_0}\right)^2 + 1 \approx \left(\frac{R_f}{R_0}\right)^2 \ln\left(\frac{R_f}{R_0}\right)^2 - \left(\frac{R_f}{R_0}\right)^2 = \frac{4kP_C}{\mu R_0^2}t. \tag{19}$$

R_f is the postion of the expanding liquid front and R_0 is the radius of the entrance, which in their analysis must be circular. Using the relationship between polar and elliptical coordinates defined by

$$r^2 = x^2 + y^2 = a^2(\cosh^2\eta\cos^2\psi + \sinh^2\eta\sin^2\psi), \tag{20}$$

one can write Eq. (19) in terms of η_f. Tracing the position of the liquid front along the y axis, we obtain

$$\frac{R_f^2}{R_0^2} = \frac{a^2}{R_0^2}\sinh^2\eta_f + 1. \tag{21}$$

The term 1 on the right-hand side of the above equation is added to ensure that $R_f/R_0 \geqslant 1$. Inserting (21) into Eq. (19) describes the position of the liquid front (along the y axis) as a function of time:

$$\left(\sinh^2\eta_f + \frac{R_0^2}{a^2}\right)\ln\left(\sinh^2\eta_f + \frac{R_0^2}{a^2}\right) - \sinh^2\eta_f = \frac{4kP_C}{\mu a^2}t = 4\tilde{t}. \tag{22}$$

The factor R_f^2/a^2 can be found from the condition that entrances for both circular and elliptical cases are the same. For $0 \leqslant \psi \leqslant \pi$ this condition reads

$$2a = \pi R_0 \quad \text{or} \quad \frac{a}{R_0} = \frac{\pi}{2}. \tag{23}$$

For large η_f we have

$$\cosh^2\eta_f \to \frac{\exp(2\eta_f)}{4}, \quad \sinh^2\eta_f \to \frac{\exp(2\eta_f)}{4} \tag{24}$$

and

$$\frac{R_f^2}{R_0^2} = \frac{a^2}{R_0^2}\frac{\exp(2\eta_f)}{4}(\cos^2\psi + \sin^2\psi) = \frac{a^2}{R_0^2}\frac{\exp(2\eta_f)}{4}. \tag{25}$$

Then the right-hand side of Eq. (19) becomes

$$\frac{a^2}{R_0^2}\left\{\frac{\exp(2\eta_f)}{4}\ln\left[\frac{a^2}{R_0^2}\frac{\exp(2\eta_f)}{4}\right] - \frac{\exp(2\eta_f)}{4}\right\} = \frac{a^2}{R_0^2}\left\{\frac{\exp(2\eta_f)}{4}\left[2\eta_f + \ln\left(\frac{a^2}{4R_0^2}\right)\right] - \frac{\exp(2\eta_f)}{4}\right\} \approx \frac{a^2}{R_0^2}\left[\frac{\eta_f\exp(2\eta_f)}{2} - \frac{\exp(2\eta_f)}{4}\right], \tag{26}$$

since $2\eta_f \gg \ln(a^2/4R_0^2)$ and therefore can be neglected. Introducing the above expression in Eq. (19) makes it identical to Eq. (18). For very large η_f one may use the approximation

$$x\ln x - x \approx \ln(x!) \approx \ln[\Gamma(x+1)], \tag{27}$$

which allows one to write the left-hand sides of Eq. (18) in a more compact form:

$$\tfrac{1}{8}\eta_f\exp(2\eta_f) - \tfrac{1}{16}\exp(2\eta_f) \approx \tfrac{1}{16}\ln[\Gamma(e^{2\eta_f}+1)]. \tag{28}$$

IV. CAPILLARY DRIVEN FLOW IN EXPANDING THREE-DIMENSIONAL POROUS MEDIA

A. Exact solution in three dimensions

For flow in 3D porous media, a general grasp of the geometry can be obtained from Figs. 1(a) and 1(b) if the graphs are revolved around their vertical axis of symmetry (the z axis in Fig. 3). The coordinates that are relevant to such a system are defined by Ref. [24] (see also Fig. 3)

$$x = a\cosh\eta\sin\theta\cos\psi, \quad y = a\cosh\eta\sin\theta\sin\psi, \quad z = a\sinh\eta\cos\theta. \tag{29}$$

Note that the variable ψ is different from the one used in the elliptic 2D case discussed above (see Fig. 3 and compare it to

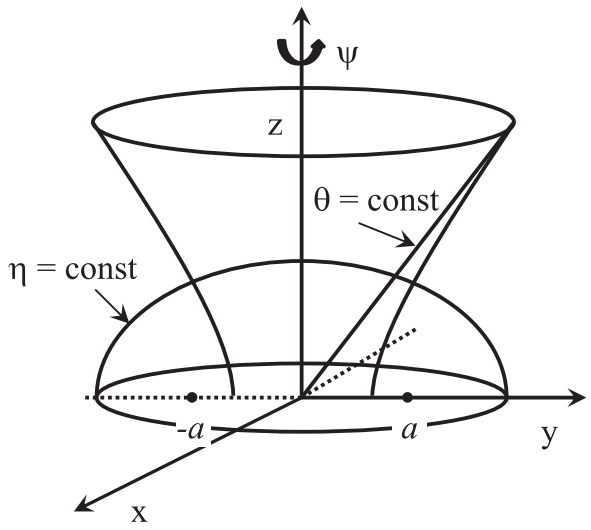

FIG. 3. Oblate spheroid coordinates, used to describe the flow in an expanding 3D porous domain. The points $-a$ and a are the foci of the oblate surface corresponding to η. Only systems with axial symmetry are considered.

Fig. 2). The Laplace equation for the flow potential, Eq. (4), has the form [24]

$$\nabla^2\varphi = \frac{1}{a^2(\cosh^2\eta - \sin^2\theta)} \times \left(\frac{\partial^2\varphi}{\partial\eta^2} + \tanh\eta\frac{\partial\varphi}{\partial\eta} + \frac{\partial^2\varphi}{\partial\theta^2} + \cot\theta\frac{\partial\varphi}{\partial\theta}\right) + \frac{1}{a^2\cosh^2\eta\sin^2\theta}\frac{\partial^2\varphi}{\partial\psi^2} = 0. \tag{30}$$

Since we consider an axis-symmetric domain, $\partial^2\varphi/\partial\psi^2 = 0$, the last term can be dropped. Additionally, there is no flow across the surface corresponding to $\theta = \pi/2$ and $\theta = -\pi/2$; hence there is no change with θ and all derivatives with respect to the polar angle are zero. Therefore Eq. (30) can be significantly simplified to

$$\frac{d^2\varphi}{d\eta^2} + \tanh\eta\frac{d\varphi}{d\eta} = 0. \tag{31}$$

This equation describes concentric oblate surfaces that correspond to the flow potential $\varphi(\eta)$. The boundary conditions for capillary driven flow are identical to those given by Eq. (8):

$$\varphi = \varphi_0 = -\frac{k}{\mu}P_C \quad \text{at} \quad \eta = 0, \quad \varphi = 0 \quad \text{at} \quad \eta = \eta_f. \tag{32}$$

The solution for the flow potential is then

$$\varphi = \varphi_0\left\{1 - \frac{\arctan[\tanh(\eta/2)]}{\arctan[\tanh(\eta_f/2)]}\right\}. \tag{33}$$

Note that for $\eta_f \to \infty$ the above expression becomes

$$\varphi = \varphi_0\left\{1 - \frac{4\arctan[\tanh(\eta/2)]}{\pi}\right\}, \tag{34}$$

which means that in the 3D case we have a finite asymptotic result on an infinite domain which is not true for the one- and two-dimensional cases.

The liquid velocity profile in the 3D porous region has only an η component, which is

$$v_\eta = \frac{1}{a(\cosh^2\eta - \sin^2\theta)^{1/2}}\frac{\partial\varphi}{\partial\eta} = \frac{kP_C}{2\mu a\cosh\eta(\cosh^2\eta - \sin^2\theta)^{1/2}\arctan[\tanh(\eta_f/2)]}. \tag{35}$$

The velocity of the front is

$$v_{\eta_f} = \frac{1}{a(\cosh^2\eta_f - \sin^2\theta)^{1/2}}\left(\frac{\partial\varphi}{\partial\eta}\right)_{\eta=\eta_f} = \frac{kP_C}{2\mu a\cosh\eta_f(\cosh^2\eta_f - \sin^2\theta)^{1/2}\arctan[\tanh(\eta_f/2)]}. \tag{36}$$

The velocity is formally expressed in terms of the spatial and temporal variables by

$$v_{\eta_f} = a(\cosh^2\eta_f - \sin^2\theta)^{1/2}\frac{d\eta_f}{dt}. \tag{37}$$

Hence, combining (36) and (37) one derives

$$\int_0^{\eta_f(t)}(\cosh^2\eta_f' - \sin^2\theta)\arctan\left[\tanh\left(\frac{\eta_f'}{2}\right)\right]\cosh\eta_f' d\eta_f' = \frac{kP_C}{2\mu a^2}t = \frac{\tilde{t}}{2}. \tag{38}$$

After integration we obtain a relationship between the front position η_f and scaled time $\tilde{t}$:

$$\frac{1}{3}\arctan\left[\tanh\left(\frac{\eta_f}{2}\right)\right][2 + 3\cos(2\theta) + \cosh(2\eta_f)]\sinh(\eta_f) - \frac{1}{6}[1 + 3\cos(2\theta)]\ln[\cosh(\eta_f)] - \frac{1}{12}[\cosh(2\eta_f) - 1] = \tilde{t}. \tag{39}$$

The front velocity is then obtained by introducing the calculated time dependence of η_f in Eq. (36) or (37). The volumetric flux is obtained from

$$U(\tilde{t}) = \int_A \mathbf{v}\cdot\mathbf{n}dA = \frac{kP_C}{\mu a}\frac{a^2}{\arctan\left\{\tanh\left[\frac{\eta_f(t)}{2}\right]\right\}}\int_0^{2\pi}d\psi\int_0^{\theta_0}\sin\theta d\theta = \frac{2\pi akP_C(1-\cos\theta_0)}{\mu\arctan\left\{\tanh\left[\frac{\eta_f(t)}{2}\right]\right\}}. \tag{40}$$

For a fully open entrance ($\theta_0 = \pi/2$),

$$U(\tilde{t}) = \frac{2\pi akP_C}{\mu\arctan\left\{\tanh\left[\frac{\eta_f(t)}{2}\right]\right\}}. \tag{41}$$

B. Asymptotic results for small and large η_f

For short times and small values of η_f and $\theta = 0$ Eq. (39) simplifies to

$$\frac{\eta_f^2}{2} = \tilde{t}. \tag{42}$$

The long-time, large η_f, asymptotic result can be derived for Eq. (39) using the same arguments as above [see Eq. (18)] and also noting that $\arctan[\tanh(\eta_f/2)] \to \pi/4$. The result is

$$\frac{\pi}{4}\frac{\exp(3\eta_f)}{12} = \tilde{t}. \tag{43}$$

For large η_f the front shape should approach that of an expanding sphere. The latter can be derived from Eq. (4) written in the form

$$\frac{1}{r^2}\frac{d}{dr}\left(r^2\frac{d\varphi}{dr}\right) = 0, \tag{44}$$

together with the following boundary conditions:

$$r = R_0, \quad \varphi = \varphi_0 = -\frac{k}{\mu}\Delta P, \quad \Delta P = P_C, \qquad r = R_f, \quad \varphi = 0. \tag{45}$$

Then the solution for the potential is (see also Ref. [16])

$$\varphi = \varphi_0\frac{R_fR_0}{R_f - R_0}\left(\frac{1}{r} - \frac{1}{R_f}\right). \tag{46}$$

It is interesting to point out that in the case of 3D radial flow, there is a finite solution for $\varphi(r)$ even if R_f is at infinity. In this case

$$\varphi = \varphi_0 \frac{R_0}{r}. \tag{47}$$

The radial velocity is then

$$v_r = \frac{\partial \varphi}{\partial r} = -\varphi_0 \frac{R_f R_0}{R_f - R_0} \frac{1}{r^2} = \frac{R_f R_0}{R_f - R_0} \frac{k P_C}{\mu} \frac{1}{r^2}. \tag{48}$$

At $r = R_f$

$$v_{R_f} = \frac{dR_f}{dt} = \frac{R_0}{R_f(R_f - R_0)} \frac{k P_C}{\mu}. \tag{49}$$

Hence the time-dependent position of the moving front is given by

$$\int_{R_0}^{R_f} \frac{R_f'(R_f' - R_0)}{R_0^3} dR_f' = \frac{R_f^3}{3R_0^3} - \frac{R_f^2}{2R_0^2} + \frac{1}{6} = \frac{a^2}{R_0^2}\tilde{t}. \tag{50}$$

The radial coordinate in 3D oblate spheroid coordinates is

$$\begin{aligned} r^2 &= x^2 + y^2 + z^2 \\ &= a^2(\cosh^2\eta \sin^2\theta \cos^2\psi + \cosh^2\eta \sin^2\theta \sin^2\psi \\ &\quad + \sinh^2\eta \cos^2\theta) \\ &= a^2(\cosh^2\eta \sin^2\theta + \sinh^2\eta \cos^2\theta). \end{aligned} \tag{51}$$

At the front $\eta = \eta_f$ and for large η_f we use the approximations $\cosh^2\eta_f \approx \exp(2\eta_f)/4$ and $\sinh^2\eta_f \approx \exp(2\eta_f)/4$. Hence

$$\frac{R_f^2}{R_0^2} = \frac{a^2}{R_0^2} \frac{\exp(2\eta_f)}{4}, \tag{52}$$

and Eq. (50) becomes

$$\begin{aligned} &\frac{R_f^3}{3R_0^3} - \frac{R_f^2}{2R_0^2} + \frac{1}{6} \\ &= \frac{a^3}{3R_0^3} \frac{\exp(3\eta_f)}{8} - \frac{a^2}{2R_0^2} \frac{\exp(2\eta_f)}{4} + \frac{1}{6} = \frac{a^2}{R_0^2}\tilde{t}, \quad \text{or} \\ &\frac{a}{R_0} \frac{\exp(3\eta_f)}{24} - \frac{\exp(2\eta_f)}{8} + \frac{R_0^2}{6a^2} = \tilde{t}. \end{aligned} \tag{53}$$

Keeping only the leading order term in Eq. (53) and expressing the ratio a/R_0 using Eq. (23) we obtain

$$\frac{\pi}{2} \frac{\exp(3\eta_f)}{24} = \tilde{t}, \tag{54}$$

which is identical to Eq. (43).

V. RESULTS AND DISCUSSION

A. Transport in two-dimensional porous media

Two effects govern the liquid transport in an expanding 2D porous region. Both of them follow from the mass conservation of the incompressible liquid. The first one follows from the mass conservation and is due to the liquid distribution over an ever-increasing space (or area). This effect leads to an apparent decrease in the velocity of the moving front. At the same time the liquid travels less distance per unit time, which lowers the friction resistance while the capillary force increases due to the expansion of the front. The combination of the two effects slows down the linear velocity and facilitates the bulk flow rate in an expanding porous material. Figures 4(a) and 4(b) show the dependence of the liquid front position and linear velocity of capillary driven liquid flow in two-dimensional porous regions. The solid lines correspond to the case depicted in Fig. 1(a) (the entrance has finite dimensions). The plot was derived from Eq. (13) setting $\psi = \pi/2$, i.e., the flow along the y axis is traced (see Fig. 2). It is compared to the LW power-law case [10,11] of nonexpanding porous material which maintains constant cross sectional dimension [dashed line; see also Eqs. (16) and (17)], as well as to the case of

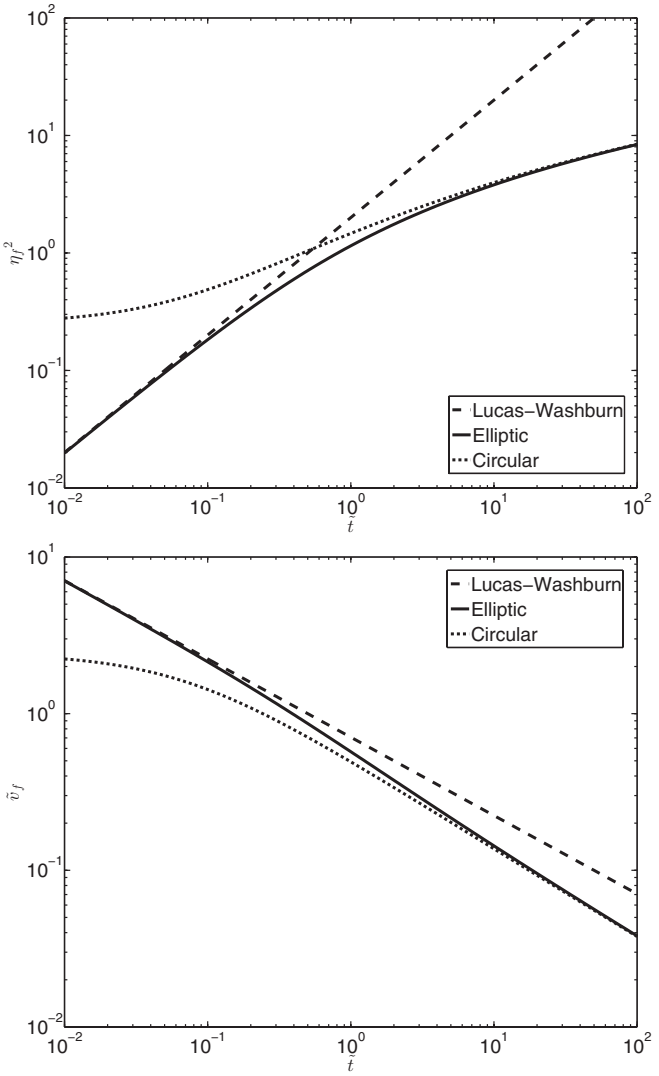

FIG. 4. (a) Position of the liquid front in an expanding 2D porous material as a function of time [see Eq. (13)] (solid line). The dashed line corresponds to the nonexpanding LW result [see Eq. (16)]. The dotted line represents the result for an expanding circular front [see Eq. (19)]. (b) Velocity of the liquid front for capillary motion in expanding 2D porous material. The solid line corresponds to the flow depicted in Fig. 1(a) [see also Eqs. (11) and (13)]. The dashed line shows the LW while the dotted line shows the 2D radial flows.

radial flow [17] [see Eq. (19)]. At short times the front position shows a power-law increase similar to the LW solution. This is due to the fact that the effect of the expansion is weak for short distances, the liquid has not spread too much, and the streamlines are almost parallel. As time progresses, however, the expansion effect increases and the distance traveled by the front in the expanding porous domain decreases in comparison with the nonexpanding LW case because liquid has also moved to the sides to form the elliptically shaped front. For long times the front becomes less elliptical and more circular and the solution for the front position asymptotically approaches that for an expanding circle given by the dotted line in Fig. 4(a) [see Eqs. (18) and the discussion thereafter]. Hence, the LW [10,11] solution and the circular expansion result obtained by Hyväluoma *et al.* [17] represent the 2D limiting cases of no expansion and maximum expansion, respectively. Our result given by Eq. (13) describes the entire time behavior including two limiting cases as well as the intermediate case, as seen from Fig. 4(a). The latter applies to a range of more than two orders of magnitude of the scaled time.

The time dependence of the linear velocity of the liquid front is shown in Fig. 4(b). The solid line corresponds to our solution given by Eq. (11) in combination with Eq. (13). The dashed line is the LW result [10,11] and the dotted line is that for the radial flow when R_f/R_0 or, equivalently, η_f are large [17]. Clearly the velocity drops with time for all the cases but at different rates. If the porous region does not expand, then the reason for the velocity decrease is due to the increase of the length of liquid penetration. This length contributes to the viscous resistance and hence, slows down the motion. If the liquid travels in an expanding material (like the examples outlined in Fig. 1) the front motion is also slowed by the fact that liquid is diverted sideways into the available expanding space. The effect of the expansion is strongest in the case of pure radial flow. At short times our solution is close to that for a nonexpanding medium and asymptotically approaches the one for radial flow at very long times.

It is interesting to examine the dependence of the bulk (volumetric) flow rate since it is a measure of the ability of the porous material to absorb liquid. An important practical application exploiting this ability is to drive fluids in devices and materials using capillary action instead of an external power source [4]. The solid line in Fig. 5 shows the change of the bulk flow rate with time calculated from Eq. (41). Since we are considering a 2D domain, the bulk flow rate is calculated per unit length in the direction normal to the plane of the flow. Again, for comparison both the nonexpanding LW and the radial expanding cases (for large η_f) are shown. Both are obtained in a similar way by multiplying the liquid velocity at the front by its length. Clearly an expanding porous material has better capabilities of absorbing liquids; as is evident in the plots, the bulk flow rate decreases much slower with time in comparison with the nonexpanding case.

B. Transport in three-dimensional porous media

The effect of expansion is stronger when it occurs in three dimensions. The reason is that there is more space available for the liquid to occupy as it moves forward driven

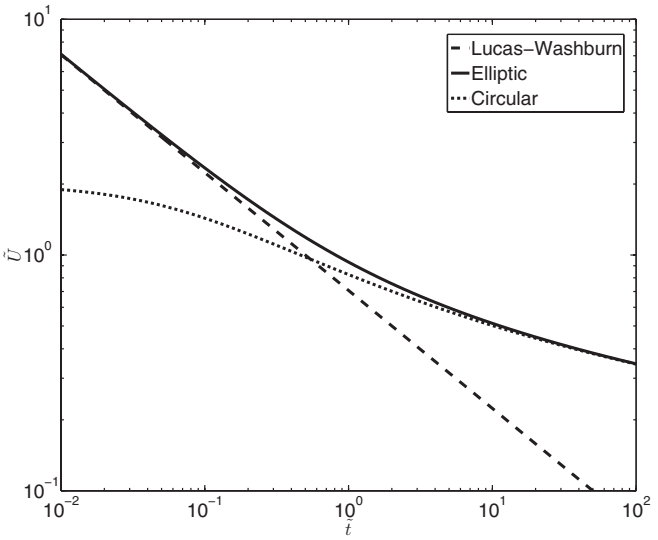

FIG. 5. Bulk flow rate vs time for expanding 2D porous materials. The solid line corresponds to the flow depicted in Fig. 1(a) [see Eqs. (15) and (13)]. The dashed line shows the LW while the dotted line shows the 2D radial flows for large η_f.

by capillary pressure. The calculations presented below are for a fully opened medium where $\theta = \pi/2$ (see Fig. 3). The entrance has a circular shape. The flow along the y axis is traced, which corresponds to $\theta = 0$. Figure 6(a) shows the position of the fluid front as a function of the elapsed time. The solid line corresponds to the solution in oblate spheroid coordinates given by Eq. (39) (i.e., the fluid enters the porous material through a circular entrance with finite dimensions) and it is compared to the nonexpanding case (dashed line) and the expansion in spherical symmetry for large R_f/R_0 [or η_f—see Eq. (54)]. At short times the expansion effect is insignificant while at long times the behavior approaches that of an expanding spherical front. Similarly to the 2D case, our solution interpolates between these two limiting cases and provides a correct description for the cases where the liquid enters the 3D expanding porous material through an entrance with a finite size.

The linear velocity of the advancing liquid front is shown in Fig. 6(b). The effect of the expansion on the front velocity resembles a 2D case [see Fig. 4(b)] but is more pronounced because of the spreading of the liquid over a larger front area. That leads to greater reduction of the velocity of the moving liquid front.

The bulk volumetric velocity is presented in Fig. 7. It should be emphasized that the 3D expanding case allows for a solution where fluid will keep entering the porous material through the circular entrance. This is also evident from Eq. (41) which for time and $\eta_f \to \infty$ becomes

$$\tilde{U}_\infty = \frac{\mu U_\infty}{2\pi a k P_C} = \frac{4}{\pi}. \tag{55}$$

This result implies that 3D porous media can be used as capillary pumps to drive fluids in devices. This cannot be accomplished if the porous material does not expand, or the expansion is two dimensional (see also the discussion below).

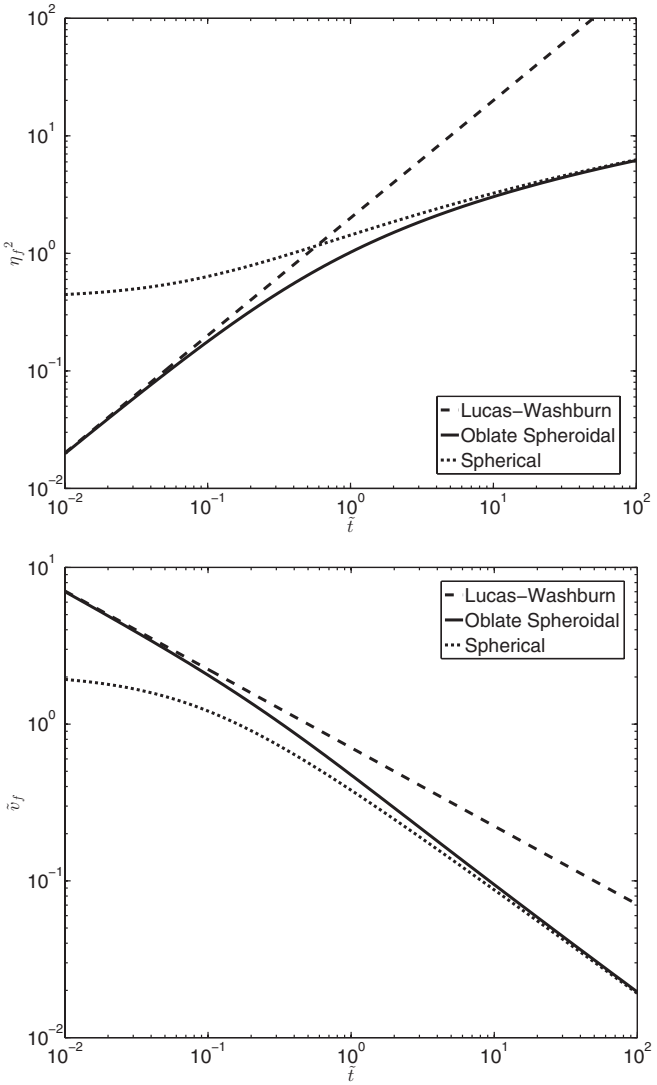

FIG. 6. (a) Liquid front position as a function of the elapsed time in a 3D expanding porous material. The solid line corresponds to the solution in oblate spheroid coordinates, the dashed line is the LW nonexpanding case, and the dotted line is the solution for spherical expansion at large η_f. (b) Linear velocity of the moving liquid front in a 3D porous material. The solid line represents the solution for an oblate spheroid front, the dashed line is for the LW solution, and the dotted line corresponds to the asymptotic case of an expanding spherical front.

The actual rate of drawing liquid in, however, will depend on parameters such as the average pore size, liquid viscosity, and pore wetting ability, and may turn out in many cases to be too low (see experimental results in Xiao *et al.* [16]).

Since the asymptotic result (55) follows from the dimensionality of the system, one may expect that a similar relationship exists for the pure radial (spherical) transport (see Fig. 7). Indeed, using Eq. (48) we can find the linear velocity at the entrance where $r = R_0$. To obtain the bulk flow rate one needs to multiply the result by the area of the entrance which we assume to be hemispherical in order to better compare to the oblate spheroid case discussed above. Thus the asymptotic

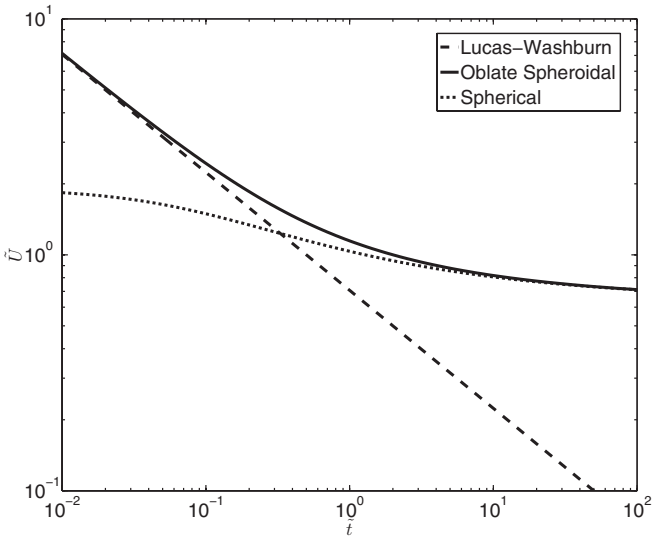

FIG. 7. Bulk flow in a 3D porous medium. The solid line shows the result for oblate spheroid symmetry, the dashed line corresponds to the LW case, and the dotted line represents the spherical case.

($R_f \to \infty$) expression reads

$$\tilde{U}_\infty = \frac{\mu U_\infty}{2\pi R_0 k P_C} = 1. \tag{56}$$

Hence, if the system is 3D, stationary solutions are possible, which is generally the case for Laplace equations in infinite or semi-infinite spaces and processes such as heat transfer or diffusion [25].

C. Effect of porous media dimensionality

The dimensionality of the porous media is extremely important for the flow rate. There is no expansion of the advancing fluid front in the case of 1D transport (which is represented by the LW case [10,11]) and the linear velocity (as well as the bulk flow rate) drops as $1/\sqrt{t}$. At the other extreme, the 3D case allows for a solution even for $\eta_f \to \infty$ [see Eq. (55) above]. Figure 8(a) shows a comparison for the time-dependent position of the moving liquid front for 1D, 2D (elliptical), and 3D (oblate spheroid) cases. The 1D case exhibits the farthest liquid penetration while in the 2D and 3D cases the distance is much shorter. The rate of liquid motion also decreases with the dimensionality of the flow [see Fig. 8(b)]. This is due to distribution of the advancing liquid over greater space. The cross sectional area that the fluid moves through does not change in the 1D case, increases linearly with distance in the 2D case, and increases quadratically in the 3D case. Since the liquid is incompressible it can cover shorter distances per unit time for the two- and particularly the three-dimensional cases. It is, however, very different for the bulk flow rate (see Fig. 9). The volume absorbed per unit time by the porous domain decreases the fastest for the 1D flow. The decrease in the bulk flow rate for the 2D expanding case is lower and for the 3D case it levels off to a steady state [see Eq. (55) above]. The reason is the bulk flow rate is slowed down by the viscous resistance which increases with the length of the traveled path. The latter is greatest in the 1D case, shorter in the 2D case, and shortest in the 3D case.

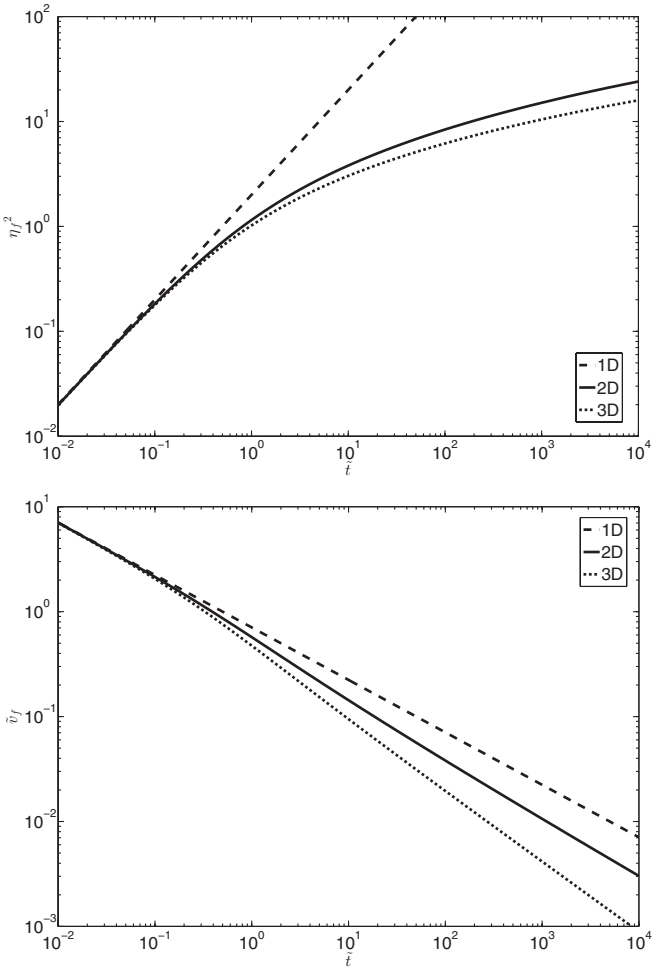

FIG. 8. (a). Liquid front position vs time in 1D (dashed line), 2D (solid line), and 3D (dotted line) cases. (b) Linear velocity of the liquid front vs time in 1D (dashed line), 2D (solid line), and 3D (dotted line) cases.

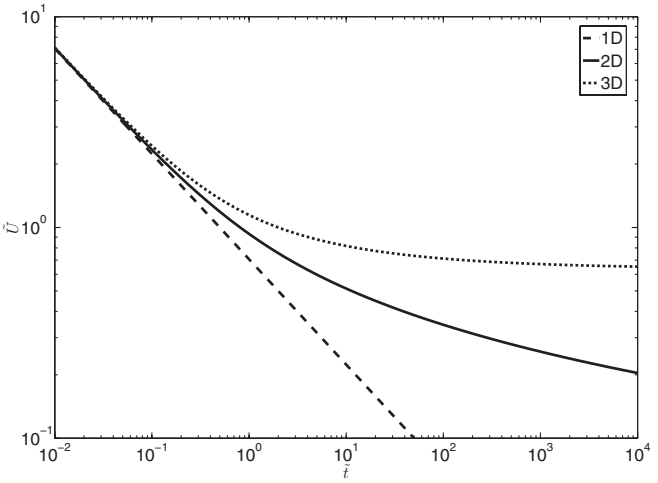

FIG. 9. Bulk liquid flow vs time in 1D (dashed line), 2D (solid line), and 3D (dotted line) cases.

VI. CONCLUSIONS

We derived solutions for potential capillary driven liquid flow in 2D and 3D expanding porous media. The selection of suitable coordinate systems allows for simplification of the mass balance expressions to ordinary differential equations that can be exactly solved. The obtained solutions for expanding 2D and 3D porous materials are different from the well-known Lucas-Washburn solution describing liquid motion in nonexpanding material geometries. The functional forms of the time dependence of the front position and velocity are more complicated if the porous domain is expanding. At the same time the liquid linear velocity is lower, which is due to spreading of the incompressible liquid over an ever-increasing domain.

The bulk flows display a qualitative difference in the 1D, 2D, and 3D cases. It decreases the fastest if the porous domain does not expand, less in the 2D expanding domain, and least in the 3D domain. In fact the 3D case can reach a steady state for the bulk flow into the porous material. This makes it suitable to use in driving fluids through devices using capillary forces and without the need of an external power source.

ACKNOWLEDGMENTS

This work was funded by NSF CAREER (Grant No. CBET 0844645) and DOE-EPSCoR Implementation Program (Grant No. DE-FG02-08ER46530).

[1] T. D. Wheeler and A. D. Stroock, Nature **455**, 208 (2008).
[2] E. M. Fenton, M. R. Mascarenas, G. P. López, and S. S. Sibbett, ACS Appl. Mater. Interfaces **1**, 124 (2009).
[3] A. W. Martinez, S. T. Phillips, and G. M. Whitesides, Anal. Chem. **82**, 3 (2010).
[4] S. Mendez, E. M. Fenton, G. R. Gallegos, D. N. Petsev, S. Sibbett, H. A. Stone, Y. Zhang, and G. P. Lopez, Langmuir **26**, 1380 (2010).
[5] N. V. Churaev, *Liquid and Vapor Flows in Porous Bodies: Surface Phenomena*, Topics in Chemical Engineering, edited by A. Galwey, Vol. 13 (Gordon and Breach, New York, 2000).
[6] F. A. L. Dullien, *Porous Media: Fluid Transport and Pore Structure* (Academic Press, New York, 1979).
[7] S. S. D. Julio and W. H. Shallenberger, J. Hazard. Subst. Res. **3**, 6-1 (2002).
[8] J. Ge, R. Schirhagl, and R. N. Zare, J. Chem. Educ. **88**, 1283 (2011).
[9] J. M. Bell and F. K. Cameron, J. Phys. Chem. **10**, 658 (1906).
[10] R. Lucas, Kolloid Z. **23**, 15 (1918).
[11] E. W. Washburn, Phys. Rev. **17**, 273 (1921).
[12] J. Happel and H. Brenner, *Low Reynold's Number Hydrodynamics*, in Mechanics of Fluids and Transport Processes, edited by R. J. Moreau (Kluwer, Boston, 1983).
[13] C. Hall, Build. Environ. **16**, 201 (1981).
[14] M. A. Wilson, W. D. Hoff, and C. Hall, Build. Environ. **29**, 99 (1994).

[15] J. R. Philip, in *Water in the Unsaturated Zone: Proceedings of the Wageningen Symposium* (International Association for Scientific Hydrology/UNESCO, Paris, 1996).
[16] J. Xiao, H. A. Stone, and D. Attinger, Langmuir **28**, 4208 (2012).
[17] J. Hyväluoma, P. Raiskinmäki, A. Jäsberg, A. Koponen, M. Kataja, and J. Timonen, Phys. Rev. E **73**, 036705 (2006).
[18] J. R. Philip, in *Advanecs in Hydroscience*, edited by W. Chou (Academic Press, New York, 1969), p. 215.
[19] R. J. Gummerson, C. Hall, W. D. Heft, R. Hawkes, G. N. Holland, and W. S. Moore, Nature **281**, 56 (1979).
[20] B. Lavi, A. Marmur, and J. Bachmann, Langmuir **24**, 1918 (2008).
[21] E. M. Benner and D. N. Petsev (in preparation).
[22] J. O. Wilkes, *Fluid Mechanics for Chemical Engineers with Microfluidics and CFD* (Prentice Hall, New York, 2006).
[23] J. S. Rowlinson and B. Widom, *Molecular Theory of Capillarity* (Claredon Press, Oxford, 1982).
[24] P. H. Moon and D. E. Spencer, *Field Theory Handbook: Including Coordinate Systems, Differential Equations and Their Solutions* (Springer, New York, 1988).
[25] L. D. Landau and E. M. Lifshitz, *Fluid Mechanics* (Elsevier, Amsterdam, 1987).